

OPTICAL DATA PROCESSING

PACS numbers: 42.25.Fx; 42.30.Wb; 42.79.Jq
DOI: 10.1070/QE2011v041n12ABEH014673

Two-dimensional image edge enhancement by two-phonon Bragg diffraction

V.M. Kotov, G.N. Shkerdin, A.N. Bulyuk

Abstract. **A model of acousto-optic interaction is developed for describing two-phonon Bragg diffraction in a gyrotropic single TeO_2 crystal, which makes allowance for ellipticity of crystal optical eigenwaves. Formation of a two-dimensional edge of an image in the first diffraction order is explained by invoking a three-dimensional description for the wave surfaces of optical eigenwaves.**

Keywords: *acousto-optic diffraction, Bragg regime, image edge enhancement.*

1. Introduction

One important problem in optical information processing is edge enhancement of an optical image (see, for example, [1]). On the one hand, this procedure considerably reduces information arrays to be processed and, on the other hand, it preserves such important object characteristics as its shape and dimensions.

Acousto-optic (AO) interaction efficiently helps solving the problem. AO diffraction is used for enhancing both one-dimensional [2, 3] and two-dimensional edges of an optical image [4–6]. The latter case is more attractive because it directly solves the problem of obtaining the whole edge.

In [7], we for the first time investigated experimentally two-dimensional edge enhancement for an optical image by employing two-phonon Bragg diffraction with formation of the edge in the first diffraction order. In [7], the effect obtained was only qualitatively explained.

Here, we develop a model, which makes allowance for ellipticity of optical eigenwaves propagating along a TeO_2 crystal near its optical axis. This approach along with a three-dimensional consideration of the wave-vector surfaces explains formation of a two-dimensional edge in the first diffraction order.

2. Theory

In some works, the models of AO diffraction were developed with allowance made for the ellipticity of eigenwaves propagating in a TeO_2 crystal (see, for example, [8–10]). However, these papers considered one-dimensional light diffraction on an ultrasonic wave; in the strict sense, results of such consideration are inapplicable to processing two-dimensional images. In our approach, we consider two-dimensional diffraction taking into account a spatial curvature of a wave-vector surface. This helps explaining the effects observed.

The diffracted fields will be calculated starting from the wave equation for a dielectric crystal:

$$\mathrm{rot}[\mathrm{rot}\boldsymbol{E}] + \frac{1}{c^2}\frac{\partial^2 \boldsymbol{D}}{\partial t^2} = 0, \tag{1}$$

where $\boldsymbol{E}$ and $\boldsymbol{D}$ are the vectors of the electric field and induction in the crystal; c is the speed of light in vacuum. The expression for a component of the dielectric tensor ε_{ik} entering into the material equation $D_i = \varepsilon_{ik}E_k$, where D_i and E_k are the components of vectors $\boldsymbol{D}$ and $\boldsymbol{E}$, respectively, is written in the form (see, for example, [11])

$$\varepsilon_{ik} = \varepsilon^0_{ik} + \mathrm{i}e_{ikl}G_l - \varepsilon^0_{il}\varepsilon^0_{km}p_{lmnj}u_{nj}. \tag{2}$$

Here, ε^0_{ik} are the components of unperturbed dielectric function; G_l are the components of an axial gyration vector; e_{ikl} is the Levi – Civita symbol; p_{lmnj} are the components of a photoelasicity tensor; u_{nj} are the components of a crystal strain tensor related to the ultrasonic wave (the additives to the dielectric function due to gyrotropy and photoelasticity are assumed small).

The components of the gyration vector may be expressed in terms of components of gyration pseudo-tensor G_{ij}: $G_i = G_{ij}s_j$, where s_j are the components of a unit vector $\boldsymbol{s}$ of a plane wave propagating in parallel with the wave vector $\boldsymbol{k}$ ($\boldsymbol{k} = k\boldsymbol{s}$). Further calculations will refer to a uniaxial crystal of tellurium dioxide (TeO_2), which has a point symmetry group 422. In the basic system of coordinates of paratellurite we have $\varepsilon^0_{xx} = \varepsilon^0_{yy} = \varepsilon_1$, $\varepsilon^0_{zz} = \varepsilon_3$, $G_{xx} = G_{yy} = G_{11}$ and $G_{zz} = G_{33}$. We assume that an electromagnetic wave propagates across the crystal at sufficiently small angles with respect to the optical axes, in which case the effect of gyrotropy is important.

Calculation of AO interaction [solving wave equation (1)] is simpler if one uses the coupled-mode approach with slowly varying wave amplitudes. Without an ultrasonic wave, a solution for the electric induction vector $\boldsymbol{D}(\boldsymbol{r})$ for every propagation direction $\boldsymbol{s}$ is given by a linear combination of two orthonormal elliptically polarised eigenmodes:

$$\boldsymbol{D}(\boldsymbol{r}) = B_1\boldsymbol{b}_1\exp(\mathrm{i}k_1\boldsymbol{s}\boldsymbol{r}) + B_2\boldsymbol{b}_2\exp(\mathrm{i}k_2\boldsymbol{s}\boldsymbol{r}), \tag{3}$$

where B_1 and B_2 are the constants responsible for the contributions of each mode into the induction:

V.M. Kotov, G.N. Shkerdin, A.N. Bulyuk V.A. Kotelnikov Institute of Radio Engineering and Electronics, Fryazino Branch, Russian Academy of Sciences, pl. Acad. Vvedenskogo 1, 141190 Fryazino, Moscow region, Russia; e-mail: vmk277@ire216.msk.su

Received 15 June 2011; revision received 20 September 2011
Kvantovaya Elektronika **41** (12) 1109–1113 (2011)
Translated by N.A. Raspopov

$$\boldsymbol{b}_1 = \frac{\boldsymbol{e}_1 + \mathrm{i}\rho\boldsymbol{e}_2}{\sqrt{1+\rho^2}}; \qquad \boldsymbol{b}_2 = \frac{\boldsymbol{e}_2 + \mathrm{i}\rho\boldsymbol{e}_1}{\sqrt{1+\rho^2}};$$

$\boldsymbol{e}_1$ and $\boldsymbol{e}_2$ are the unit vectors directed along main axis of a central cross section of the crystal indicatrix by a wave-front plane, which is determined by vector $\boldsymbol{s}$ (vector $\boldsymbol{e}_1$ is directed along the short axis of the ellips); ρ is the ellipticity of eigenmode polarisation, i.e., the ratio of short to long axis lengths for the polarisation ellipse; k_1 and k_2 are the absolute values of the wave vectors for eigenwaves. Ellipticity ρ and the absolute values k_1 and k_2 of the wave vectors are given by known relationships [11–13]. A similar to (3) expression holds for the electric field vector $\boldsymbol{E}(\boldsymbol{r})$ where the ellipticity of eigenmodes in the plane of the wave front coincides with ellipticity ρ in expression (3); however, there is a small longitudinal field component.

Assume that the slow transverse sonic wave propagates in the [110] direction and causes mechanical deformations of matter perpendicular to both the crystal optical axis and direction of wave propagation. We may transfer from the basic system of coordinates [100], [010], [001] to the system of coordinates xyz with the axis $x\|[1\,\bar{1}0]$, $y\|[110]$ and $z\|[001]$. In this case, AO interaction is described by a single photoelastic constant $p_{66} = (p_{11} - p_{22})/2$, where p_{11}, p_{22} are the components of photoelastic tensor in double-index notation. Consider double AO interaction describing zero and second diffraction orders by the solution branches with the greater refraction factor; then, with neglected gyrotropy, the optical radiation will be represented by extraordinary rays. The first diffraction order we will describe by the solution branch with the smaller refraction factor, in which case radiation may be presented as ordinary rays. The expressions for the electric fields in the diffraction orders $\boldsymbol{E}_{mi}(\boldsymbol{r})$ are written in the form

$$\boldsymbol{E}_{mi}(\boldsymbol{r}) = V_{mi}(z)\boldsymbol{b}_{mi}\exp[\mathrm{i}k_{mz} + \mathrm{i}k_{0x}x + \mathrm{i}(k_{0y} + mq)y - \mathrm{i}\omega_m t], \quad (4)$$

where $m = 0, 1, 2$ is the diffraction order number; i is the mode number ($i = 1$ corresponds to the slower mode, $i = 2$ corresponds to the faster mode); k_{0x} and k_{0y} are the wave vector projections for the incident electromagnetic wave onto the axis x and y; k_{mz} is the z-component of the wave vector for the corresponding eigenmode described by the vector $\boldsymbol{b}_{mi}$; $\omega_m = \omega + m\Omega$; ω and Ω are the angular frequencies for the electromagnetic and ultrasonic waves, respectively.

If there is an ultrasonic wave, the amplitudes of eigenmodes satisfying Bragg synchronism conditions are slow functions of coordinates. By neglecting the longitudinal components of the electric field, we may derive a system of reduced equations for the amplitudes issuing from the orthogonality of eigenmodes in the wave-front plane (see, for example, [12]). The resulting system of equations for the slow electric field amplitudes in diffraction orders $V_{mi}(z)$ has the form:

$$\frac{\mathrm{d}V_{01}}{\mathrm{d}z} = \mathrm{i}\gamma_1^*\exp[\mathrm{i}(k_{1z} - k_{0z})z]V_{12}, \quad (5)$$

$$\frac{\mathrm{d}V_{12}}{\mathrm{d}z} = \mathrm{i}\gamma_1\exp[\mathrm{i}(k_{0z} - k_{1z})z]V_{01} + \mathrm{i}\gamma_2\exp[\mathrm{i}(k_{2z} - k_{1z})z]V_{21}, \quad (6)$$

$$\frac{\mathrm{d}V_{21}}{\mathrm{d}z} = \mathrm{i}\gamma_2^*\exp[\mathrm{i}(k_{1z} - k_{2z})z]V_{12}, \quad (7)$$

where $\gamma_{1,2} = k^2\Delta\varepsilon_{1,2}f_{1,2}/(2k_{0z})$ are the coupling constants; $\Delta\varepsilon_1 = -\frac{1}{2}q\varepsilon_1^2 p_{66}A\mathrm{e}^{-\mathrm{i}\varphi}$; $\Delta\varepsilon_2 = \Delta\varepsilon_1^*$; A and q are the amplitude and absolute value of the ultrasound wave vector; φ is the phase of the ultrasound wave; $f_1 = (\boldsymbol{d}_{1x} + \boldsymbol{d}_{1y})\tilde{\boldsymbol{b}}_1$ and $f_2 = (\boldsymbol{d}_{2x} + \boldsymbol{d}_{2y})\tilde{\boldsymbol{b}}_1^*$ are the coefficients describing influence of eigenwave ellipticity on the diffraction process:

$$\boldsymbol{d}_{1x} = \frac{\mathrm{i}\rho_0\boldsymbol{e}_{10y} + \boldsymbol{e}_{20y}}{\sqrt{1+\rho_0^2}}; \quad \boldsymbol{d}_{1y} = \frac{\mathrm{i}\rho_0\boldsymbol{e}_{10x} + \boldsymbol{e}_{20x}}{\sqrt{1+\rho_0^2}};$$

$$\boldsymbol{d}_{2x} = \frac{\mathrm{i}\rho_2\boldsymbol{e}_{12y} + \boldsymbol{e}_{22y}}{\sqrt{1+\rho_2^2}}; \quad \boldsymbol{d}_{2y} = \frac{\mathrm{i}\rho_2\boldsymbol{e}_{12x} + \boldsymbol{e}_{22x}}{\sqrt{1+\rho_2^2}};$$

$$\tilde{\boldsymbol{b}}_1 = \frac{\boldsymbol{e}_{11} + \mathrm{i}\rho_1\boldsymbol{e}_{21}}{\sqrt{1+\rho_1^2}};$$

vector $\boldsymbol{e}_{10}$ denotes vector $\boldsymbol{e}_1$ for the zero diffraction order, $\boldsymbol{e}_{11}$ refers to the first order diffraction; vectors $\boldsymbol{e}_{20}$, $\boldsymbol{e}_{21}$, etc., are similarly defined; $\boldsymbol{e}_{10y}$ is the projection of vector $\boldsymbol{e}_{10}$ onto the y, axes, $\boldsymbol{e}_{10x}$ – onto the x axes and so on; ρ_0, ρ_1, ρ_2 are the ellipticities of eigenmodes for zero, first, and second orders, respectively.

Expressions for $f_{1,2}$ are rather cumbersome even at small angles between the radiation propagation direction and crystal optical axes. They are noticeably simpler in the following two limiting cases: at $k_{0x} = 0$, i.e., when the electromagnetic wave propagates in the plane $x = 0$, in which the optical axes and the wave vector of the ultrasound wave reside; and when we neglect the small incident angles and their influence is only taken into account in the calculation of eigenmode ellipticity. In the case of $k_{0x} = 0$ (the interacting optical rays lie in the plane $x = 0$) the expression for $f_{1,2}$ takes the form

$$f_{1,2} = \frac{\cos\beta_{0,2} + \rho_{0,2}\rho_1\cos\beta_1}{\sqrt{(1+\rho_{0,2}^2)(1+\rho_1^2)}}, \quad (8)$$

where $\beta_{0,1,2}$ are the angles between the optical axes and the rays, diffracted into zero, first, and second orders [9].

By neglecting small incident angles and taking into account the fact that the electromagnetic wave may propagate in an arbitrary plane we may write the expression for $f_{1,2}$ in the form

$$f_{1,2} = \frac{\cos(\theta_{0,2} + \theta_1)(1 + \rho_{0,2}\rho_1) + \mathrm{i}(\rho_{0,2} + \rho_1)\sin(\theta_{0,2} + \theta_1)}{\sqrt{(1+\rho_{0,2}^2)(1+\rho_1^2)}}, \quad (9)$$

where $\theta_{0,1,2}$ are the angles between the vector $\boldsymbol{e}_1$ and x axes for the radiation diffracted into zero, first, and second orders. Note that these angles, generally speaking, are not negligible even at small incident angles. For example, for the first diffraction order, by denoting the angle between the projection of vector $\boldsymbol{k}_0$ onto plane $y = 0$ and z axes as φ_0, and the angle between vector $\boldsymbol{k}_0$ and its projection onto the plane $y = 0$ as φ_{01} we arrive at $\theta_0 = -\arctan(\sin\varphi_0/\tan\varphi_{01})$, which entails $\theta_0 = 0$ at $\varphi_0 = 0$, at an arbitrary angle φ_{01} (except for $\varphi_{01} = 0$). In this case, we have $k_{0x} = 0$. Next, at $\varphi_{01} = 0$ we have $\theta_0 = \pm\pi/2$ at arbitrary angle φ_0 (except for $\varphi_0 = 0$). Here we have $k_{0y} = 0$. From (9) follows

$$|f_{1,2}| = \sqrt{\frac{(1 + \rho_{0,2}\rho_1)^2 - \sin^2(\theta_{0,2} + \theta_1)(1 - \rho_{0,2}^2)(1 - \rho_1^2)}{(1+\rho_{0,2}^2)(1+\rho_1^2)}},$$

and in the case where the polarisation of eigenmodes is almost circular, we obtain

$$|f_{1,2}| \approx \frac{1+\rho_{0,2}\rho_1}{\sqrt{(1+\rho_{0,2}^2)(1+\rho_1^2)}}. \quad (10)$$

Expressions for the coupling constants $\gamma_{1,2}$ may be written in the form $\gamma_{1,2} = [\nu/(2L)]f_{1,2}$, where ν is the Raman–Nath parameter and L is the length of AO interaction. For linear and circular polarisations we obtain $f_{1,2} = 1$, and Eqns (5) – (7) transfer to well known expressions (see, for example, [10, 14]).

Note that system of equations (5) – (7) describes an experimental situation where the intensities of the radiation diffracted into different orders, determined by the functions $|V_{mi}(z)|^2$ are measured.

Using the expressions obtained we performed numerical calculations taking into account the two-dimensional character of AO diffraction near the optical axes of a TeO_2 crystal. Three-dimensional wave surfaces of light waves were described by the expressions used in [7]. The parameters for a single TeO_2 crystal were taken from [15, 16]. By solving (5) – (7) in a standard way (see, for example, [17]) we obtain normalised electric field amplitudes V_{01}, V_{12} and V_{11} for the radiation diffracted into zero, first, and second orders, respectively. For $f_{1,2}$ we used expression (9).

Figure 1 shows a calculated two-dimensional transfer function for the first diffraction order under the assumption that it coincides with the distribution $|V_{12}|$. It was assumed that optical radiation at the wavelength of 0.63 μm diffracts on the slow acoustic wave (which propagates in a TeO_2 crystal at the velocity of 0.617×10^5 cm s^{-1}) with the frequency close to that of two-phonon resonance. The angular dimensions in Fig. 1 correspond to ~2°×2°. The Raman–Nath parameter ν was taken equal to $\sim 4\sqrt{2}\pi$, which corresponded to the acoustic power in our experiment. The length of AO interaction was L = 6 mm. The image in Fig. 1 is a set of elliptical fringes, which result from the interference of first order diffraction rays with the rays diffracted to the first order from zero and second orders. Domains with substantial anomalies are seen in the fringe image. The fringes in the domains are strongly distorted and their distribution becomes actually two-dimensional. One such domain is marked by a square and is separately presented in Fig. 2, its angular dimension is ~0.5°×0.5°. If the whole domain is used as a mask for optical Fourier processing of images then it will present a two-dimensional spatial low-cut filter.

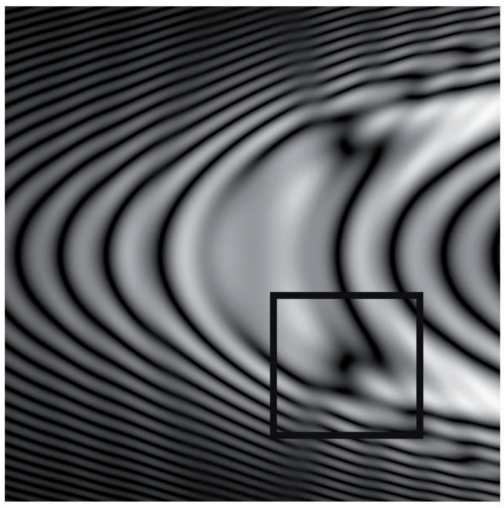

Figure 1. Transfer function for the first diffraction order $|V_{12}|$ formed as the result of two-phonon Bragg diffraction. Dark regions correspond to minimum field distribution and light regions correspond to maximum distribution.

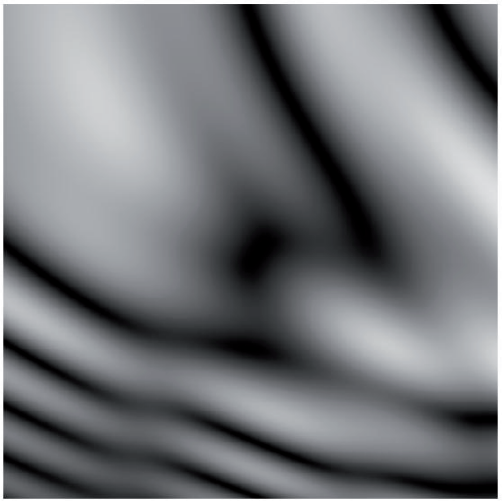

Figure 2. Domain of transfer function selected in Fig. 1.

Note that the elliptical character of optical rays taken into account substantially affects the characteristics of the transfer functions. For comparison, in Fig. 3 the same transfer function is shown as in Fig. 2; however, in the approximation of strongly circular polarisations of optical rays. One can see that the two-dimensional character of the transfer function vanishes, the curves become straighten, which prevents obtaining a two-dimensional edge of the image. In other lim-

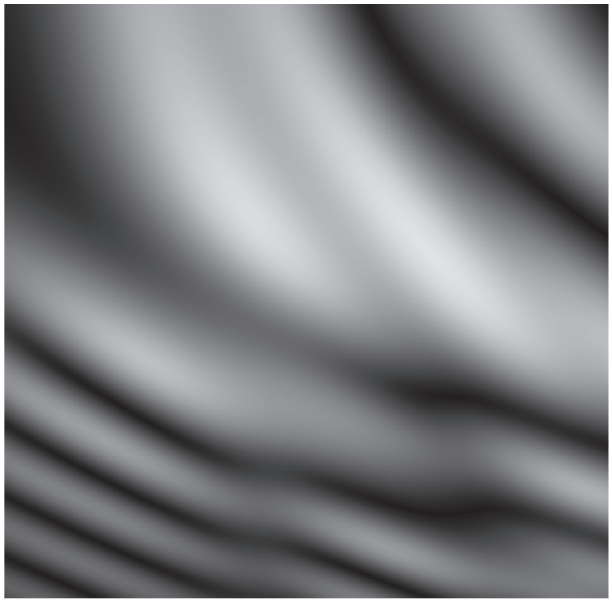

Figure 3. Transfer function formed by rays with circular polarisations.

iting case with linear polarisations of the optical rays, the transfer function is a set of weakly bent curves (Fig. 4). In the middle of Fig. 4, one can see anomalies in the curve behavior; however, the two-dimensional character is not observed. We also failed to obtain a two-dimensional edge. In Fig. 5, numerical results of Fourier processing are presented for images of a rectangular and circle with employment of the transfer function $|V_{12}|$ (see Fig. 2). One can see that in the both cases sufficiently clear two-dimensional edges are formed. Hence, generally, the mask presented by the distribution from Fig. 2 can be used as a two-dimensional spatial low-cut filter despite its sufficiently large inhomogeneity. As was mentioned, the masks obtained with neglected ellipticity of light wave polarisation (see Figs 3 and 4) cannot enhance a two-dimensional edge.

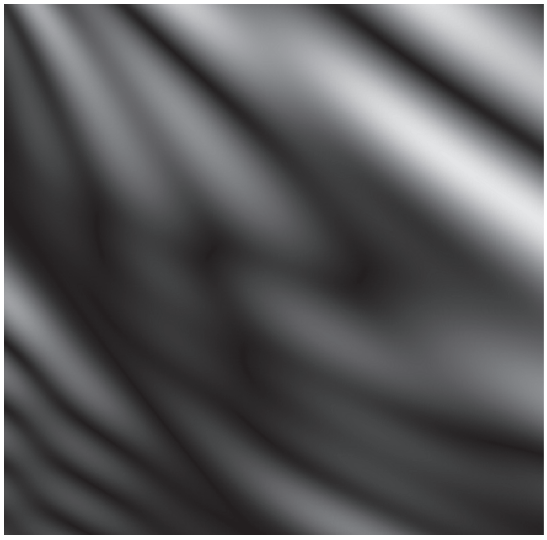

Figure 4. Transfer function formed by rays with linear polarisations.

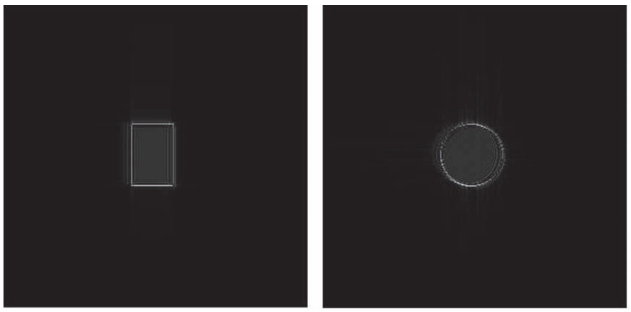

a b

Figure 5. Results of computer Fourier processing for rectangular and circular hole images with the transfer function shown in Fig. 2.

3. Experiment and discussion of results

Some experiments concerning formation of a two-dimensional edge for an optical image were described in [7]. In the present work, some additional experiments have been performed. Edge enhancement by two-phonon Bragg diffraction is specific in that it is necessary to choose the mask position in the angular space. Indeed, one can see in Fig. 1 that the mask domain shifts from the position of exact Bragg synchronism (image centre) in both horizontal and vertical angular directions. Actually, it is necessary to detune from the exact Bragg synchronism angle in both the diffraction plane and orthogonal plane. The experimental setup sufficiently well described in [7] was taken as a basis. The initial image was either a rectangular hole of the size 1×1.5 mm or a circular hole 1.0 mm in diameter. The holes were illuminated from one side by wide radiation of a He–Ne laser ($\lambda = 0.63$ μm), which then passed to an input lens. Behind the lens, an AO cell made of TeO_2 was placed and then there was a second lens. The focal distances of both the lenses were 16 cm. Results of optical Fourier processing were observed on a screen placed behind the second lens. The voltage applied to a piezoelectric transducer was 5.0 V, and the frequency of an ultrasound wave was 35.5 MHz. By angular adjustment in the diffraction plane and in the orthogonal plane we obtained a two-dimensional edge of the image in the first order.

Figure 6 shows photographs of screen images. One can see that a clear two-dimensional edge is formed in the first diffraction order. In other words, the experiment confirms that two-phonon AO diffraction makes it possible to enhance a two-dimensional edge of an image in the first diffraction order in accordance with the theoretical conclusions.

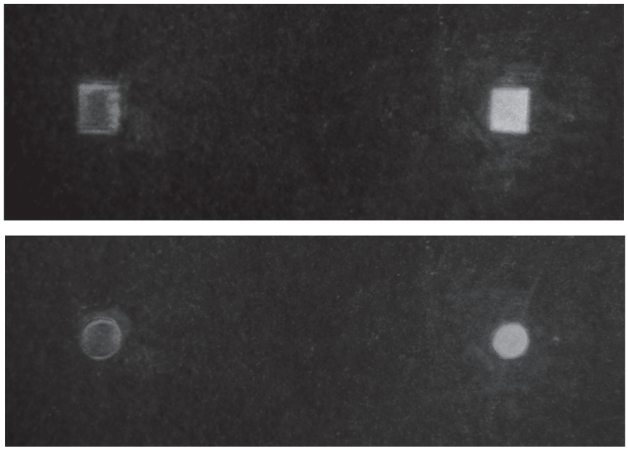

Figure 6. Photographs of rectangular and circular holes after experimental Fourier processing. Right images correspond to the zero diffraction order and left images correspond to the first diffraction order.

4. Conclusions

From the above consideration we may conclude:

(i) The theory of two-phonon Bragg AO diffraction is developed, which takes into account both the surface curvature of eigenwaves and ellipticity of polarisation for propagating rays.

(ii) It is shown that the theory developed is capable of explaining formation of two-dimensional edge for an optical image in the first diffraction order in the course of two-phonon diffraction in TeO_2, whereas a model neglecting ellipticity of eigenwaves cannot explain the effect.

(iii) Experiments on forming image edges for rectangular and circular holes well agree with the numerical results obtained by Fourier processing of those images.

Acknowledgements. The work was supported by the Russian Foundation for Basic Research (Grant Nos 09-07-00047 and

12-07-00233) and by the Grant of the RF President for support of Leading Scientific Schools (Grant No. NSh-3317.2010.9).

References

1. Young T.Y., Fu K.-S. (Eds) *Handbook of Pattern Recognition and Image Processing* (New York: Acad. Press, 1986).
2. Athale R.A., van der Gracht J., Prather D.W., Mait J.N. *Appl. Opt.*, **4**, 276 (1995).
3. Kotov V.M., Shkerdin G.N., Shkerdin D.G., Kotov E.V. *Radiotekh. Elektron.*, **54**, 747 (2009).
4. Balakshy V.I., Voloshinov V.B., Babkina T.M. Kostyuk D.E. *J. Mod. Optics*, **52**, 1 (2005).
5. Balakshy V.I., Mantsevich C.N. *Opt. Spektrosk*., **103**, 831 (2007).
6. Balakshy V.I., Kostyuk D.E. *Appl. Opt*., **48**, C24 (2009).
7. Kotov V.M., Averin S.V., Shkerdin G.N., Voronko A.I. *Kvantovaya Elektron.*, **40**, 368 (2010) [*Quantum Electron*., **40**, 368 (2010)].
8. Belyi V.N., Shepelevich V.V. *Opt. Spektrosk*., **52**, 842 (1982).
9. Rakovskii V.Yu., Shcherbakov A.S. *Zh. Tekh. Fiz.*, **60**, 107 (1990).
10. Xu J., Stroud R. *Acousto-Optic Devices: Principles, Design, and Applications* (New York: John Wiley & Sons, 1992).
11. Landau L.D., Lifshitz E.M. *Electrodynamics of Continuous Media* (Oxford: Pergamon Press, 1984).
12. Yariv A., Yeh P. *Optical Waves in Crystals* (New York: Wiley, 1984; Moscow: Mir 1987).
13. Sirotin Yu.I., Shaskol'skaya M.P. *Osnovy kristallofiziki* (Principles of Crystal physics) (Moscow: Nauka, 1975)].
14. Balakshy V.I., Parygin V.N., Chirkov L.E. *Fizicheskie osnovy akustooptiki* (Physical Principles of Acousto-optics) (Moscow: Radio i svyaz', 1985).
15. Shaskol'skaya M.P. (Ed.) *Akusticheskie kristally* (Acoustic Crystals) (Moscow: Nauka, 1982).
16. Kizel' V.A., Burkov V.I. *Girotropiya kristallov* (Crystal Gyrotropy) (Moscow: Nauka, 1980).
17. Kotov V.M. *Opt. Spektrosk*., **79**, 307 (1995)].